ARCHIVES OF ELECTRICAL ENGINEERING VOL. 72(4), pp. 871 –893 (2023)

DOI 10.24425/aee.2023.147416

Optimal size and location of dispatchable distributed generators in an autonomous microgrid using Honey Badger algorithm

THAM X. NGUYEN, ROBERT LIS ✉

Faculty of Electrical Engineering, Wrocław University of Science and Technology
Wybrzeże Wyspiańskiego 27, 50-370 Wrocław, Poland
e-mail: {tham.nguyen/✉Robert.Lis}@pwr.edu.pl

(Received: 21.03.2023, revised: 07.06.2023)

Abstract: The paper presents a honey badger algorithm (HB) based on a modified backward-forward sweep power flow method to determine the optimal placement of droop-controlled dispatchable distributed generations (DDG) corresponding to their sizes in an autonomous microgrid (AMG). The objectives are to minimise active power loss while considering the reduction of reactive power loss and total bus voltage deviation, and the maximisation of the voltage stability index. The proposed HB algorithm has been tested on a modified IEEE 33-bus AMG under four scenarios of the load profile at 40%, 60%, 80%, and 100% of the rated load. The analysis of the results indicates that Scenario 4, where the HB algorithm is used to optimise droop gains, the positioning of DDGs, and their reference voltage magnitudes within a permissible range, is more effective in mitigating transmission line losses than the other scenarios. Specifically, the active and reactive power losses in Scenario 4 with the HB algorithm are only 0.184% and 0.271% of the total investigated load demands, respectively. Compared to the base scenario (rated load), Scenario 4 using the HB algorithm also reduces active and reactive power losses by 41.86% and 31.54%, respectively. Furthermore, the proposed HB algorithm outperforms the differential evolution algorithm when comparing power losses for scenarios at the total investigated load and the rated load. The results obtained demonstrate that the proposed algorithm is effective in reducing power losses for the problem of optimal placement and size of DDGs in the AMG.

Key words: autonomous microgrid, dispatchable distributed generator, droop control, modified backward-forward sweep, voltage stability index

1. Introduction

The rapid development of distributed and dispersed generation (DG) has been enormously integrating into the power grid. DG can be installed near local loads, which helps to reduce power loss in lines, enhance power quality, and improve the overall system reliability [1,2]. According to IEEE Std 1547™-2018 [3], DGs operating in a microgrid (MG) in autonomous mode (grid-off) offer numerous benefits compared to the grid-on mode. In addition to the advantages mentioned above, they also improve energy security, facilitate the easy expansion of the local network, and more. However, the improper placement and capacity of DGs in an autonomous microgrid (AMG) will distract from all the aforementioned advantages. Therefore, it is essential to determine the appropriate size and location of DGs in an AMG to fully realise the benefits they offer.

Metaheuristic and multi-objective evolutionary algorithms, along with their variants, have proven to be effective in tackling complex and nonlinear problems, and they are widely applied in real-world applications. For example, a modified version of the differential evolution algorithm (DE) has been introduced to estimate the parameters of the Jiles-Atherton hysteresis model [4]. The elephant clan optimisation algorithm has been employed to solve the optimal dynamic load flow problem in an AMG [5]. The non-dominated sorting genetic algorithm II (NSGA II) has been used to detect the optimal siting of capacitor banks (CB) [6] and DGs [7]. In addition, an improved version of NSGA II has been developed to address the environmental-economic dispatch problem in an IEEE 30-bus network [8].

The proper placement and/or capacity of distributed energy resources (DERs) in an AMG can be categorised into two main groups. The first group focuses on determining the optimal size of the DERs. The second group addresses the simultaneous optimisation of both the capacity and location of the DERs.

The appropriate size of the DERs in an AMG can be identified using various well-known methods. In [9], a weighted aggregated grey wolf optimiser (GWO) is utilised to optimise the size of dispatchable DG (DDG), renewable DG and battery energy storage systems (BESS) in a 33-bus AMG. The objective was to minimise annual operation and maintenance costs, power losses, and annual emissions. In [10], the capacity of DDGs, renewable DGs and CBs in a 33-bus AMG has been optimised using a hybrid technique called fuzzy and multi-objective particle swarm optimisation (PSO). The goal of this study was to reduce active power loss, total operation cost, and emissions.

In earlier studies, several techniques were introduced for the optimal sizing and siting of DGs in AMGs. In the case of the AMG 33-bus system, which has been transformed from the existing 33-bus distribution network (DN), the proper location and capacity of the DGs were determined using genetic algorithm (GA) and PSO to minimise active power loss [11]. In [12], the authors proposed a fuzzy method combined with NSGA II to simultaneously optimise the size and position of DGs in an AMG, with the aim of reducing voltage and frequency deviations. Minimising active power loss, voltage deviation, and frequency deviation in the AMG 38-bus system was achieved using mixed-integer nonlinear programming (MINP) in [13]. Optimal placement and sizing of DGs in the AMG have also been addressed in other studies, such as the use of mixed integer linear programming [14] for placement and sizing, the reconfigurable network and positioning of DGs [15] to mitigate active power loss in the AMG, and a chaotic GWO algorithm [16] to determine the size and location of DDGs, renewable DGs and CBs in the AMG 69-bus system, with the aim of minimising power losses, improving the voltage stability index (VSI). In [17], the teaching learning-based optimisation algorithm was used to identify the appropriate rating and position of multiple diesel generators, renewable DGs, and BESS in the AMG 17-bus system, with the goal of reducing power losses, initial investment cost, operational and maintenance cost, and replacement cost. In [18] a hybrid technique was developed that combined harmonic search, GA and fuzzy method to determine the optimal sizing and location of DDGs and wind turbines in the AMG 69-bus system, resulting in the optimisation of the cost of DDG fuel, the VSI and the total voltage deviation. In [19] a hybrid method involving GA and MINP was used to find the optimal placement and size of double-fed induction generators driven by wind turbines, diesel generators, and CBs in the AMG 69-bus system, with the objective of minimising the total expected cost, operating and maintenance cost, and annualized capital.

The optimal placement and size of dump loads in AMGs have also received significant attention from researchers [20, 21]. In [20], the authors proposed the use of a modified backward-forward sweep (MBFS) load flow method in [22], together with PSO, NSGA II, and a fuzzy method to mitigate voltage and frequency deviations in the AMG. In [21], an improved version of the MBFS method combined with a mixed integer distributed ant colony is introduced to minimise power losses as well as voltage and frequency deviations in the AMG.

A honey badger algorithm (HB) is a robust optimisation technique that was introduced by Hashim *et al.* in 2022 [23]. It has been applied to various real-world applications, such as optimal load balancing in wireless 5G [24], parameter estimation of photovoltaic systems [25], minimisation of voltage deviation in an AMG [26], and parameter identification of the Hammerstein-Wiener model [27]. In this study, the HB algorithm, based on the MBFS method described in [22], is developed to detect the appropriate size and placement of droop-controlled DDGs in the AMG 33-bus system. To assess the performance of the HB algorithm in the proposed model, the results obtained using the HB algorithm were compared with the base scenario presented in Table 4 of [22] and the differential evolution algorithm.

The rest of this paper is arranged as follows. Sections 2 and 3 are the mathematical model formulation and constraints, respectively. The proposed solutions that are used to address the problem model are introduced in Section 4. The test system data and study scenarios are presented in Section 5. Section 6 describes the results and the discussion. Conclusions and further research are described in Section 7.

2. Problem formulation

An objective function is for mitigating active power loss F_1, considering the reduction of reactive power loss F_2 and total bus voltage deviation F_3, as well as maximising VSI F_4.

$$\min F_1\left(\boldsymbol{x}_{\text{place}}, \boldsymbol{x}_{\text{size}}, \boldsymbol{x}_{V_{\text{ref}}}\right), \tag{1}$$

$$\boldsymbol{x}_{\text{place}} = [Pla_{\text{DDG1}}, Pla_{\text{DDG2}}, \ldots, Pla_{\text{DDG}i}], \quad \boldsymbol{x}_{\text{size}} = [m_{p1}, m_{p2}, \ldots, m_{pi}, n_{q1}, n_{q2}, \ldots, n_{qi}],$$

$$\boldsymbol{x}_{V\,\text{ref}} = [|V_{\text{ref1}}|, |V_{\text{ref2}}|, \ldots, |V_{\text{ref}i}|], \quad i \in \{1, 2, \ldots, N_{\text{DDG}}\},$$

where: $\boldsymbol{x}_{\text{place}}, \boldsymbol{x}_{\text{size}}$ and $\boldsymbol{x}_{V_{\text{ref}}}$ are the optimal location, droop gains, and reference voltage magnitude vectors of the DDGs, respectively; $Pla_{\text{DDG}i}$ is the i-th DDG siting, and its droop gains are represented by m_{pi} and n_{qi}; the reference voltage magnitude of the i-th DDG is $|V_{\text{ref}i}|$; N_{DDG} denotes the number of DDGs.

a. Power loss in lines

$$F_1 = \sum_{t=1}^{T} \sum_{i=1}^{N_{br}} R_i I_i^2 , \tag{2}$$

$$F_2 = \sum_{t=1}^{T} \sum_{i=1}^{N_{br}} X_i I_i^2 , \tag{3}$$

where: R_i and X_i denote the resistance and reactance of the i-th branch, respectively; I_i is the current flowing through the i-th branch; T represents the whole investigated time; N_{br} is the number of branches; t denotes the investigated time.

b. Total nodal voltage deviation

The total bus voltage deviation can be calculated as in [28], as follows:

$$F_3 = \sum_{t=1}^{T} \sum_{i=1}^{N} |1 - V_i|, \tag{4}$$

where: N is the number of buses and $|V_i|$ represents the voltage magnitude of the i-th bus.

c. Voltage stability index

To assess the operational capability of the AMG, the VSI is used to determine a stable voltage value for all buses [29], which is described in Eq. (5). As stated in [18], the AMG is considered to be in a stable state if and only if the $\text{VSI}_{(i+1)}$ value at time t is greater than zero.

$$\text{VSI}_{(i+1)}(t) = |V_i|^4 - 4(P_{i+1}X_i - Q_{i+1}R_i)^2 - 4(P_{i+1}R_i + Q_{i+1}X_i)|V_i|^2, \tag{5}$$

$$F_4 = \text{VSI}_{(i+1)}(t), \quad i \in \{1, 2, \ldots, N\}, \tag{6}$$

where: P_{i+1} and Q_{i+1} are the total active and reactive power load fed through the $(i+1)$-th bus, respectively; $\text{VSI}_{(i+1)}$ is the voltage stability index of the $(i+1)$-th bus at time t.

3. Constraints

a. Power balance equations

$$\begin{aligned} &\sum_{i=1}^{N_{\text{DDG}}} \frac{1}{m_{pi}} (\omega(t) - \omega_{\text{ref}}) + \sum_{i=1}^{N_{\text{DDG}}} P_{\text{DDG}io} - \sum_{i=1}^{N} P_{Li}(t) \\ &\qquad = \sum_{i=1}^{N} \sum_{j=1}^{N} |V_i(t)||V_j(t)|Y_{ij}(t) \cos\left(\delta_i(t) - \delta_j(t) - \theta_{ij}(t)\right), \end{aligned} \tag{7}$$

$$\begin{aligned} &\sum_{i=1}^{N_{\text{DDG}}} \frac{1}{n_{qi}} (|V_i(t)| - |V_{\text{ref}i}(t)|) + \sum_{i=1}^{N_{\text{DDG}}} Q_{\text{DDG}io} - \sum_{i=1}^{N} Q_{Li}(t) \\ &\qquad = \sum_{i=1}^{N} \sum_{j=1}^{N} |V_i(t)||V_j(t)|Y_{ij}(t) \sin\left(\delta_i(t) - \delta_j(t) - \theta_{ij}(t)\right), \end{aligned} \tag{8}$$

where: m_{pi} and n_{qi} represent the P and Q droop coefficients of the i-th DDG at time t respectively; $|V_{\mathrm{ref}i}|$ denotes the reference voltage magnitude of the i-th DDG at time t; $|V_i|$ and $|V_j|$ are the operating voltage magnitudes of the i-th and j-th buses at time t; ω_{ref} is the reference frequency; ω signifies the operating frequency at time t; $P_{\mathrm{DDG}io}$ and $Q_{\mathrm{DDG}io}$ denote the active and reactive reference points of the i-th DDG, respectively [22], and can be set at zero value [30]; P_{Li} and Q_{Li} denote the load demand of the i-th bus at time t; δ_i and δ_j represent the voltage's phase angles of the i-th and j-th buses at time t; θ_{ij} and Y_{ij} are the admittance's phase angle and magnitude between the j-th bus and the i-th bus at time t respectively.

b. Inequality constraints

b.1. The operating frequency and voltage magnitude

The operating frequency and voltage magnitude should be retained within a predefined range as follows:

$$\omega^{\min} \le \omega(t) \le \omega^{\max}, \tag{9}$$

$$|V^{\min}| \le |V_i(t)| \le |V^{\max}|. \tag{10}$$

$\omega^{\min}$ and $\omega^{\max}$ are given 0.99 pu and 1.0 pu, respectively. $|V^{\min}|$ and $|V^{\max}|$ are given 0.95 pu and 1.05 pu, respectively, where the operating voltage magnitude has upper and lower limits denoted by $|V^{\max}|$ and $|V^{\min}|$, while the operating frequency has upper and lower bounds denoted by $\omega^{\max}$ and $\omega^{\min}$.

b.2. Power limit of the dispatchable distributed generation

$$P_{\mathrm{DDG}i}(t) \le P_{\mathrm{DDG}i}^{\max}, \tag{11}$$

$$Q_{\mathrm{DDG}i}(t) \le Q_{\mathrm{DDG}i}^{\max}, \tag{12}$$

where: $P_{\mathrm{DDG}i}$ and $Q_{\mathrm{DDG}i}$ denote the active and reactive power generated by the i-th DDG at time t respectively; $P_{\mathrm{DDG}i}^{\max}$ and $Q_{\mathrm{DDG}i}^{\max}$ are the upper thresholds of the active and reactive power of the i-th DDG.

b.3. The reference voltage magnitude and droop gains of the DDG

$$\left|V_{\mathrm{ref}}^{\min}\right| \le |V_{\mathrm{ref}i}(t)| \le \left|V_{\mathrm{ref}}^{\max}\right|, \quad i \in \{1, 2, \ldots, N_{\mathrm{DDG}}\}, \tag{13}$$

$|V_{\mathrm{ref}}^{\min}|$ and $|V_{\mathrm{ref}}^{\max}|$ are given 1.0 pu and 1.02 pu, respectively.

$$m_{pi}^{\min} \le m_{pi}(t) \le m_{pi}^{\max}, \quad i \in \{1, 2, \ldots, N_{\mathrm{DDG}}\}, \tag{14}$$

$$n_{qi}^{\min} \le n_{qi}(t) \le n_{qi}^{\max}, \quad i \in \{1, 2, \ldots, N_{\mathrm{DDG}}\}, \tag{15}$$

where: $m_{pi}^{\min}$ and $n_{qi}^{\min}$ are the minimum values of the droop gains of the i-th DDG; $m_{pi}^{\max}$ and $n_{qi}^{\max}$ denote the maximum values of the droop gains of the i-th DDG; $|V_{\mathrm{ref}}^{\min}|$ and $|V_{\mathrm{ref}}^{\max}|$ represent the minimum and maximum values of the DG reference voltage magnitude, respectively.

4. Proposed solution

In this study, the two metaheuristic algorithms, which include the DE and HB algorithms based on the optimal load flow method in the AMG introduced by Hameed F. *et al*. [22], are developed to identify the size and location of DDGs in the AMG 33-bus network. The sequential performance of each method is depicted below.

4.1. Differential evolution

In 1995, Storn and Price introduced a population-based technique with simple operators such as mutation, crossover, and selection [31]. In particular, it is a robust algorithm for finding global optimisation. The details of the DE algorithm are explained as follows:

Step 1: Initialisation – to generate initial candidate solutions in the population with size N_P

$$\boldsymbol{X}_P = [\boldsymbol{x}_1, \boldsymbol{x}_2, \ldots, \boldsymbol{x}_i], \quad \boldsymbol{x}_i = \left[x_{i1}, x_{i2}, x_{i3}, \ldots, x_{ij}\right], \quad i \in \{1, 2, \ldots, N_P\}, \quad j \in \{1, 2, \ldots, D\},$$

$$\boldsymbol{x}_i = \boldsymbol{lb}_i + \boldsymbol{r}_1(\boldsymbol{ub}_i - \boldsymbol{lb}_i), \quad i \in \{1, 2, \ldots, N_P\}, \tag{16}$$

where: $\boldsymbol{X}_P$ is population of candidate solutions; $\boldsymbol{x}_i$ represents a vector of the i-th candidate solution in the population; x_{ij} is the j-th control variable of the i-th solution; D is the number of control variables; $\boldsymbol{ub}_i$ and $\boldsymbol{lb}_i$ are vectors of upper and lower limits of the search space, respectively; $\boldsymbol{r}_1$ is a vector of random values $\in (0, 1)$.

Step 2: Mutation

In each k-th generation, the mutant vector $\boldsymbol{v}_i^k$ is generated by recombining random elements from three different solution vectors: $\boldsymbol{x}_{r1}^k, \boldsymbol{x}_{r2}^k$, and $\boldsymbol{x}_{r3}^k$. Equation (17) describes a mutation strategy of the DE algorithm based on DE/rand/1/bin.

$$\boldsymbol{v}_i^k = \boldsymbol{x}_{r3}^k + F(\boldsymbol{x}_{r1}^k - \boldsymbol{x}_{r2}^k), \quad i \in \{1, 2, \ldots, N_P\}, \quad k \in \{1, 2, \ldots, G_{\max}\}, \tag{17}$$

where: F denotes a scaling factor $\in [0, 2]$, a larger value of F corresponds to an improved exploration capacity within the entire search space. Conversely, a lower value of F contributes to a faster convergence speed; $G_{\max}$ is the maximal number of generations; $\boldsymbol{r}_1$, $\boldsymbol{r}_2$ and $\boldsymbol{r}_3$ denote different randomness positive integer indices $\in [1, N_P]$ and $N_P \geq 4$.

Step 3: Crossover

Changing the mutant vector using the crossover operator will create a diversification of the population's solutions.

$$u_{ij}^k = \begin{cases} v_{ij}^k & \text{if } \text{rand}_j(0,1) \leq CR \text{ or } j \in \{1, 2, \ldots, D\} \\ x_{ij}^k & \text{otherwise} \end{cases}, \tag{18}$$

where: the j-th parameter of $\boldsymbol{u}_i^k$, $\boldsymbol{v}_i^k$ and $\boldsymbol{x}_i^k$ denotes as u_{ij}^k, v_{ij}^k and x_{ij}^k respectively; $\boldsymbol{u}_i^k$, $\boldsymbol{v}_i^k$ and $\boldsymbol{x}_i^k$ are the trial, mutant, and target vectors of the i-th solution at the k-th generation, respectively; $\text{rand}_j(0, 1)$ is a value of uniform random $\in (0, 1)$ of the j-th control variable; CR is a value of the crossover factor constant $\in (0, 1)$, with optimal values typically falling within the range of 0.4 to 1.0.

Step 4: Selection process

$$\boldsymbol{x}_i^k = \begin{cases} \boldsymbol{u}_i^k & \text{if } f(\boldsymbol{u}_i^k) \leq f(\boldsymbol{x}_i^k) \\ \boldsymbol{x}_i^k & \text{otherwise} \end{cases}, \quad f(\,) \text{ is the objective function.} \tag{19}$$

During the selection process, either solution $\boldsymbol{u}_i^k$ or $\boldsymbol{x}_i^k$ is chosen as a new member of the next generation in the population, based on a comparison of their fitness values $f(\boldsymbol{u}_i^k)$ and $f(\boldsymbol{x}_i^k)$. As the maximum generation is reached, the solution with the best fitness is selected.

4.2. Honey badger algorithm

The HB algorithm is inspired by the honey badger hunting process in nature. It is an efficient algorithm for solving engineering problems due to the exploration-exploitation balance during the search process and the global search capabilities. The sequential performance of the HB algorithm can be presented as follows:

Step 1: Initialise the number of honey badgers in the population, it is described as follows:

$$\boldsymbol{X}_H = [\boldsymbol{x}_1, \boldsymbol{x}_2, \ldots, \boldsymbol{x}_i], \quad \boldsymbol{x}_i = \left[x_{i1}, x_{i2}, x_{i3}, \ldots, x_{ij}\right], \quad i \in \{1, 2, \ldots, N_H\}, \quad j \in \{1, 2, \ldots, D_H\},$$
$$\boldsymbol{x}_i = \boldsymbol{lb}_i + \boldsymbol{r}_1 (\boldsymbol{ub}_i - \boldsymbol{lb}_i), \quad i \in \{1, 2, \ldots, N_H\}, \tag{20}$$

where: $\boldsymbol{X}_H$ denotes population of candidate solutions in the HB algorithm; $\boldsymbol{x}_i$ is a location vector of the i-th badger in the population with size N_H; x_{ij} is the j-th decision variable of the i-th solution; D_H is the number of decision variables; r_1 is a vector of random values $\in (0, 1)$; $\boldsymbol{ub}_i$ and $\boldsymbol{lb}_i$ represent vectors of upper and lower bounds of the search space, respectively.

Step 2: Intensity refers to the strength of the prey's source and the distance between the prey and the i-th badger. The mobility of each honey badger is mainly determined by the quality of its sense of smell. If the smell intensity of a badger is high, it will exhibit faster movement, whereas a lower smell intensity will result in slower movement. The quality of smell intensity, denoted as I_i can be determined using the following Eq. (21):

$$I_i = r_2 \frac{S}{4\pi d_i^2}, \quad r_2 \text{ is a random value } \in (0, 1), \tag{21}$$

$$\begin{aligned} S &= (\boldsymbol{x}_i - \boldsymbol{x}_{i+1})^2, \\ \boldsymbol{d}_i &= \boldsymbol{x}_{\text{prey}} - \boldsymbol{x}_i, \end{aligned} \tag{22}$$

where: S is a prey siting; $\boldsymbol{d}_i$ is a distance vector between the prey and the i-th badger; $\boldsymbol{x}_{i+1}$ represents a siting vector of the $(i + 1)$-th badger; $\boldsymbol{x}_{\text{prey}}$ is a prey placement vector.

Step 3: The density factor α is used to guarantee a smooth transition from an exploration state to an exploitation state. It gradually decreases as the number of iterations increases, with the aim of reducing randomisation over time.

$$\alpha = C e^{-\frac{g}{T_{\max}}}, \quad g \in \{1, 2, \ldots, T_{\max}\}, \tag{23}$$

where: C denotes a constant, which has a default value of 2 and is greater than or equal to 1; g is the current iteration; $T_{\max}$ is the maximum number of iterations.

Step 4: Update the new position of the i-th badger. This step can be simulated through two phases: the digging phase and the honey phase.

Step 4-1: In the digging strategy, the movement of the honey badger is similar to that of the heart shape, which can be built as follows:

$$\boldsymbol{x}_{i,\text{new}}^{g} = \boldsymbol{x}_{\text{prey}} + F\beta I\boldsymbol{x}_{\text{prey}} + Fr_3\alpha\boldsymbol{d}_i\left|\cos 2\pi r_4[1-\cos(2\pi r_5)]\right|, \tag{24}$$

$$F = \begin{cases} 1 & \text{if } r_6 \le 0.5 \\ -1 & \text{otherwise} \end{cases}, \quad r_6 \text{ is a random value} \in (0,1),$$

where: $\boldsymbol{x}_{i,\text{new}}^{g}$ is a new position vector of the i-th badger at the g-th iteration; F is a flag that is used to determine the search direction; β is a seeking ability of the honey badger to obtain food, with a default value of 6 and is greater than or equal to 1; I is the intensity quality; r_3, r_4 and r_5 are different random values $\in (0,1)$.

Step 4-2: In the honey strategy, a honey badger is supported by a honeyguide bird to search for food, and its new position can also be determined as follows:

$$\boldsymbol{x}_{i,\text{new}}^{g} = \boldsymbol{x}_{\text{prey}} + Fr_7\alpha\boldsymbol{d}_i\,, \quad r_7 \text{ is a random value} \in (0,1). \tag{25}$$

Step 5: To compute fitness value f_{new} of a new solution $\boldsymbol{x}_{i,\text{new}}^{g}$ and compared to fitness value f_i of a solution $\boldsymbol{x}_i^g$. If $f_{\text{new}} \le f_i$ then replace $\boldsymbol{x}_i^g = \boldsymbol{x}_{i,\text{new}}^{g}$ and $f_i = f_{\text{new}}$, where: $\boldsymbol{x}_i^g$ is the i-th solution at the g-th iteration; f_{new} and f_i are the objective functions.

Step 6: If $f_{\text{new}} \le f_i$ then compare fitness value f_{new} with f_{prey} (f_{prey} is the fitness/objective function of a solution $\boldsymbol{x}_{\text{prey}}$). If $f_{\text{new}} \le f_{\text{prey}}$ then replace $\boldsymbol{x}_{\text{prey}} = \boldsymbol{x}_{i,\text{new}}^{g}$ and $f_{\text{prey}} = f_{\text{new}}$.

Step 7: To check the stop criteria, if it is not satisfied, then repeat the steps from Step 2 to Step 6, else print the values of $\boldsymbol{x}_{\text{prey}}$ and f_{prey}.

4.3. Optimal power flow with droop-controlled dispatchable DG-based AMG

4.3.1. Load model

The active and reactive power of the electric load P_{Li} and Q_{Li} depend on the magnitude and frequency of the operating voltage, and can be mathematically represented as follows [32]:

$$\begin{aligned} P_{Li} &= P_{Lio}\left(\frac{|V_i|}{|V_o|}\right)^a \left(1 + K_{pf}(f - f_o)\right), \\ Q_{Li} &= Q_{Lio}\left(\frac{|V_i|}{|V_o|}\right)^b \left(1 + K_{qf}(f - f_o)\right), \end{aligned} \tag{26}$$

where: P_{Lio} and Q_{Lio} represent the active and reactive power of the load corresponding to the nominal voltage magnitude and frequency of the i-th bus, respectively; $|V_i|$ denotes the voltage magnitude of the i-th bus; $|V_o|$ is the nominal voltage's magnitude, while f_o signifies its corresponding frequency; f is the operating frequency; a and b denote the exponents; K_{pf} and K_{qf} are the sensitivity parameters; the values of a, b, K_{pf} and K_{qf} are determined as in [32].

4.3.2. Dispatchable distributed generation model

Most DGs that join the MG are typically equipped with an inverter. The inverter operates in two modes: the PQ inverter control mode and the voltage source inverter control mode [33]. In the PQ inverter control mode, the inverter can inject or absorb a predefined reactive and/or active power. In the voltage source inverter control mode, the inverter employs a droop operation to regulate the system's frequency and voltage. The model based on the DG droop strategy in an AMG relies on the DG and line impedances. When the inductor value predominates over the resistor value in this impedance, the model can be expressed as [22]:

$$\begin{aligned} f &= f_o + m_p\left(P_{\mathrm{DDG}} - P_{\mathrm{DDG}o}\right), \\ |V| &= |V_{\mathrm{ref}}| + n_q\left(Q_{\mathrm{DDG}} - Q_{\mathrm{DDG}o}\right), \end{aligned} \tag{27}$$

where: m_p and n_q denote the droop gains of the DDG; $|V_{\mathrm{ref}}|$ is the reference voltage magnitude of the DDG; $|V|$ represents the operating voltage magnitude of the DDG; the active and reactive power generated by the DDG are denoted by P_{DDG} and Q_{DDG}; $P_{\mathrm{DDG}o}$ and $Q_{\mathrm{DDG}o}$ are the active and reactive power set points of the DDG, respectively.

4.3.3. Load flow in an autonomous microgrid

Unlike traditional DNs [34], DGs operating in an AMG are often small in size. As a result, there is no presence of a slack bus or a reference voltage from the main grid in the system. Furthermore, the system frequency is not specified as a constant value [22]. Therefore, to control the magnitude and frequency of the AMG voltage within an acceptable range, it is necessary to have at least one DDG that uses the droop strategy [9, 33]. The MBFS method, introduced by Hameed F. *et al.* in 2017 [22], is employed to determine the proper size and location of the DG in the AMG. The sequential steps of this method are described below.

Step 1: Choose any bus in the AMG to generate a virtual bus that operates as the slack bus connecting the AMG to the assumed pseudo-grid. To simplify the computation, the first bus is chosen as the virtual bus.

Step 2: Create the initial parameters, the instantaneous voltage $V_i = 1\angle 0°$ pu with $i \in [1, N]$, $f = 1$ pu, $\Delta f = 0$, $\Delta V_1 = 0$, $m = 0$, $n = 0$, and convergence limit $\varepsilon = 10^{-4}$, where: Δf is the system frequency deviation and ΔV_1 refers to the voltage deviation at the virtual bus; m and n represent the values of the outer and inner iterations, respectively.

Step 3: Calculate the current injected into each bus I_i as follows:

$$P_{\mathrm{DDG}i} = P_{\mathrm{DDG}io} + \Delta P_{\mathrm{DDG}i}, \qquad \Delta P_{\mathrm{DDG}i} = \frac{\Delta f}{m_{pi}}, \qquad \Delta f = f - f_o, \tag{28}$$

$$Q_{\mathrm{DDG}i} = Q_{\mathrm{DDG}io} + \Delta Q_{\mathrm{DDG}i}, \qquad \Delta Q_{\mathrm{DDG}i} = \frac{\Delta V_i}{n_{qi}}, \qquad \Delta V_i = |V_i| - 1, \tag{29}$$

$$\begin{aligned} S_i &= P_i + jQ_i, \\ P_i &= P_{Li} - P_{\mathrm{DDG}i}, \\ Q_i &= Q_{Li} - Q_{\mathrm{DDG}i}, \end{aligned} \tag{30}$$

$$I_i = \left(\frac{S_i}{V_i}\right)^*, \quad i \in \{2, 3, \ldots, N\}, \tag{31}$$

where: P_i, Q_i and S_i denote the injected active, reactive, and apparent powers at the i-th bus, respectively; $\Delta P_{\mathrm{DDG}i}$ and $\Delta Q_{\mathrm{DDG}i}$ are the active and reactive power generated by the i-th DG, respectively, due to frequency deviation Δf and its terminal voltage magnitude deviation ΔV_i.

Step 4: Calculate the vector of the branch current $\boldsymbol{B}$ based on the matrix of bus injection to branch current $\boldsymbol{BIBC}$ and the vector of bus current injection $\boldsymbol{I}$ defined in [35] below:

$$[\boldsymbol{B}] = [\boldsymbol{BIBC}][\boldsymbol{I}]. \tag{32}$$

Step 5: Calculate the voltage vector $\boldsymbol{V}$ of all buses except the first bus based on the voltage vector of the first bus $\boldsymbol{V}_1$, the matrix of branch current to bus voltage $\boldsymbol{BCBV}$ and the vector of the branch current $\boldsymbol{B}$ defined in [35] below:

$$[\boldsymbol{V}] = [\boldsymbol{V}_1] - [\boldsymbol{BCBV}][\boldsymbol{B}]. \tag{33}$$

Step 6: Calculate the tolerance tol of the voltage at each bus apart from the first bus in the n-th inner iteration compared to the $(n-1)$-th inner iteration below:

$$\mathrm{tol} = \max\left|V_i^n - V_i^{n-1}\right|, \quad i \in \{2, 3, \ldots, N\}, \tag{34}$$

where $|V_i^n|$ and $|V_i^{n-1}|$ are the magnitudes of the voltage at the i-th bus of the n-th and $(n-1)$-th inner iterations, respectively.

Step 7: If the value of the tolerance tol is greater than the convergence limit ε, then gain the n-th inner iteration value by 1 and jump to step 3, otherwise jump to step 8.

Step 8: Calculate the operating frequency deviation Δf as follows:

$$\Delta f = m_{peq}\left[P_{\mathrm{DDG1}} - R(V_1 B_{j-1}^*)\right], \tag{35}$$

$$m_{peq} = \left(\sum_{i=1}^{N_{\mathrm{DDG}}} \frac{1}{m_{pi}}\right)^{-1}, \tag{36}$$

where: m_{peq} is an equivalent active power droop coefficient; P_{DDG1} denotes the active power generated by the virtual bus, and it can be given to zero value; $R(V_1 B_{j-1}^*)$ is a real part of the apparent power flowing from the virtual bus to the j-th bus; V_1 represents the voltage of the virtual bus; B_{j-1} is the branch current flowing from the virtual bus to the j-th bus.

Step 9: Update the operating frequency as follows:

$$f^{m+1} = f^m + \Delta f, \tag{37}$$

where: f^{m+1} and f^m are the operating frequency at the $(m+1)$-th and m-th outer iterations, respectively.

Step 10: Calculate the voltage deviation of the virtual bus ΔV_1 as follows:

$$\Delta V_1 = n_{qeq}\left[Q_{\mathrm{DDG1}} - I(V_1 B_{j-1}^*)\right], \tag{38}$$

$$n_{qeq} = \left(\sum_{i=1}^{N_{\mathrm{DDG}}} \frac{1}{n_{pi}}\right)^{-1}, \tag{39}$$

where: n_{qeq} is an equivalent reactive power droop coefficient; Q_{DDG1} denotes the reactive power generated by the virtual bus, and it can be given to zero value; $I(V_1 B_{j-1}^*)$ is an imaginary part of the apparent power flowing from the virtual bus to the j-th bus.

Step 11: Update the voltage magnitude of the virtual bus V_1 as follows:

$$\left|V_1^{m+1}\right| = \left|V_1^m\right| + \Delta V_1, \tag{40}$$

where: $|V_1^{m+1}|$ and $|V_1^m|$ are the voltage magnitudes of the virtual bus at the $(m+1)$-th and m-th outer iterations, respectively.

Step 12: Update the apparent power injection S_i for all the DG buses based on Eqs. (28), (29), and (30) using f^{m+1} and the instantaneous voltage V_i at the n-th inner iteration.

Step 13: Update the branch impedances as follows:

$$Z_{ij} = R_{ij} + jX_{ij}\frac{f^{m+1}}{f^m}, \tag{41}$$

where: Z_{ij} represents the branch impedance connecting the i-th bus to the j-th bus, with R_{ij} denoting the resistance and X_{ij} representing the reactance of the aforementioned branch.

Step 14: If the value ΔV_1 is greater than the convergence limit ε, then increase the value of the m-th outer iteration by 1 and jump to step 3, otherwise jump to step 15.

Step 15: Print the frequency and magnitude values of the system voltage.

5. Data from the test system and study scenarios

In this study, the IEEE 33-bus DN [36] is transformed into the AMG form by eliminating the tie-switch link between bus 1 and the substation of the main grid. The test system parameters that include the rated load and voltage are 3.715 MW and 2.3 MVAr at 12.66 kV, respectively. The test system is used to detect the proper location and size of five droop-controlled dispatchable DGs. The dispatchable DGs driven by gas turbines, natural gas fuel cells, etc. are used to meet the load requirements. The proposed model was scripted using Matlab software. Table 3 shows the power limits for the five DGs. The set of predefined parameters for the DE and HB algorithms is presented in Table 1 and Table 2, respectively. The load model parameters, such as a, b, K_{pf} and K_{qf} were set to zero. The reference points for the active and reactive power of all DGs $P_{\mathrm{DDG}o}$ and $Q_{\mathrm{DDG}o}$ were set to 0.2 pu. The load profile examined in this study included four time intervals, where the load was set at 40%, 60%, 80%, and 100% of the rated load for each interval at $t = 1, 2, 3,$ and 4.

Four study scenarios were proposed to evaluate the effectiveness of the DE and HB algorithms as follows: **Scenario 1** focused on optimising the droop gains of DGs with fixed reference voltage magnitudes of 1.0 pu. In **Scenario 2**, the droop gains of DGs were optimised while simultaneously optimising their reference voltage magnitudes within the permissible range from

1.0–1.02 pu. **Scenario 3** involved optimising both the droop gains and positioning of DGs with fixed reference voltage magnitudes of 1.0 pu. In **Scenario 4**, the droop gains and positioning of DGs were optimised while concurrently optimising their reference voltage magnitudes within the permissible range from 1.0–1.02 pu. The proper location of five DGs for Scenarios 1 and 2 was assumed to be the same as in [22] (i.e., on buses 1, 6, 13, 25, and 33).

Table 1. The setting of predefined parameters of the DE algorithm

Scenarios	$G_{\max}$	N_P	F	CR	D
1	20	30	0.2	0.5	10
2	20	30	0.2	0.5	15
3	15	20	0.2	0.5	15
4	15	20	0.2	0.5	20

Table 2. The setting of predefined parameters of the HB algorithm

Scenarios	$T_{\max}$	N_H	β	C	D_H
1	20	30	6	2	10
2	20	30	6	2	15
3	15	20	6	2	15
4	15	20	6	2	20

Table 3. Dispatchable DG power limits (kW and kvar)

Sequential DDG	$P_{\mathrm{DDG}i}^{\max}$	$Q_{\mathrm{DDG}i}^{\max}$
DG1	950	520
DG2	875	515
DG3	800	510
DG4	775	505
DG5	700	490

6. Numerical results and discussion

In this study, the rated load values were compared with the data presented in Table 4 [22], which served as the base scenario. The tuning values of the droop gains for the five DGs were analysed in four different scenarios using the DE and HB algorithms. These scenarios were based on the load profile at 40%, 60%, 80%, and 100% of the rated load. Their tuning values are illustrated in Figs. 1 and 2. The data from these figures point out that higher values of droop gains m_p and n_q led to an increase in the generated active and reactive power of DGs. Conversely, lower values of m_p and n_q resulted in a decrease in the generated powers. Furthermore, the optimal

Table 4. Values $|V_{\mathrm{ref}}|$ (pu) of DGs for Scenario 2 (percentage of the rated load – % rated load)

% rated load	DE					HB				
	DG1	**DG2**	**DG3**	**DG4**	**DG5**	**DG1**	**DG2**	**DG3**	**DG4**	**DG5**
40	1.0109	1.0190	1.0117	1.0113	1.0182	1.0105	1.0200	1.0000	1.0005	1.0200
60	1.0139	1.0127	1.0128	1.0158	1.0199	1.0124	1.0200	1.0143	1.0147	1.0200
80	1.0112	1.0188	1.0064	1.0083	1.0195	1.0156	1.0200	1.0080	1.0066	1.0200
100	1.0156	1.0146	1.0118	1.0160	1.0143	1.0137	1.0166	1.0143	1.0167	1.0168

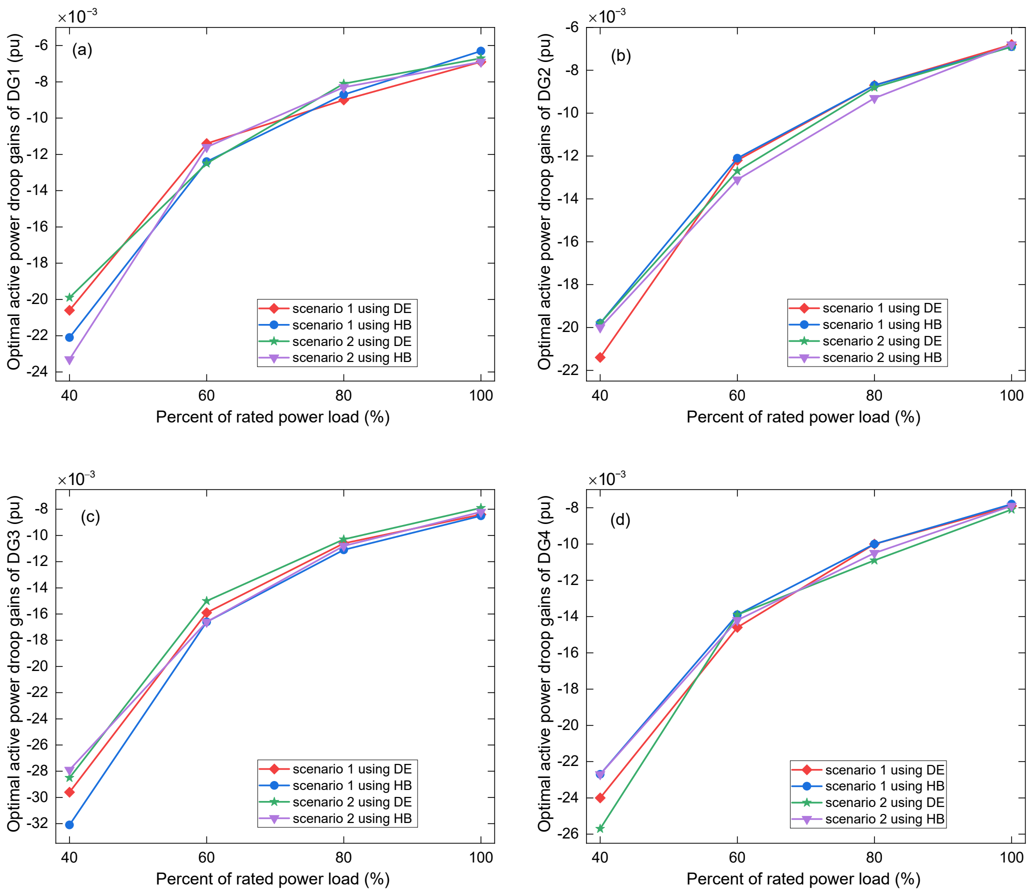

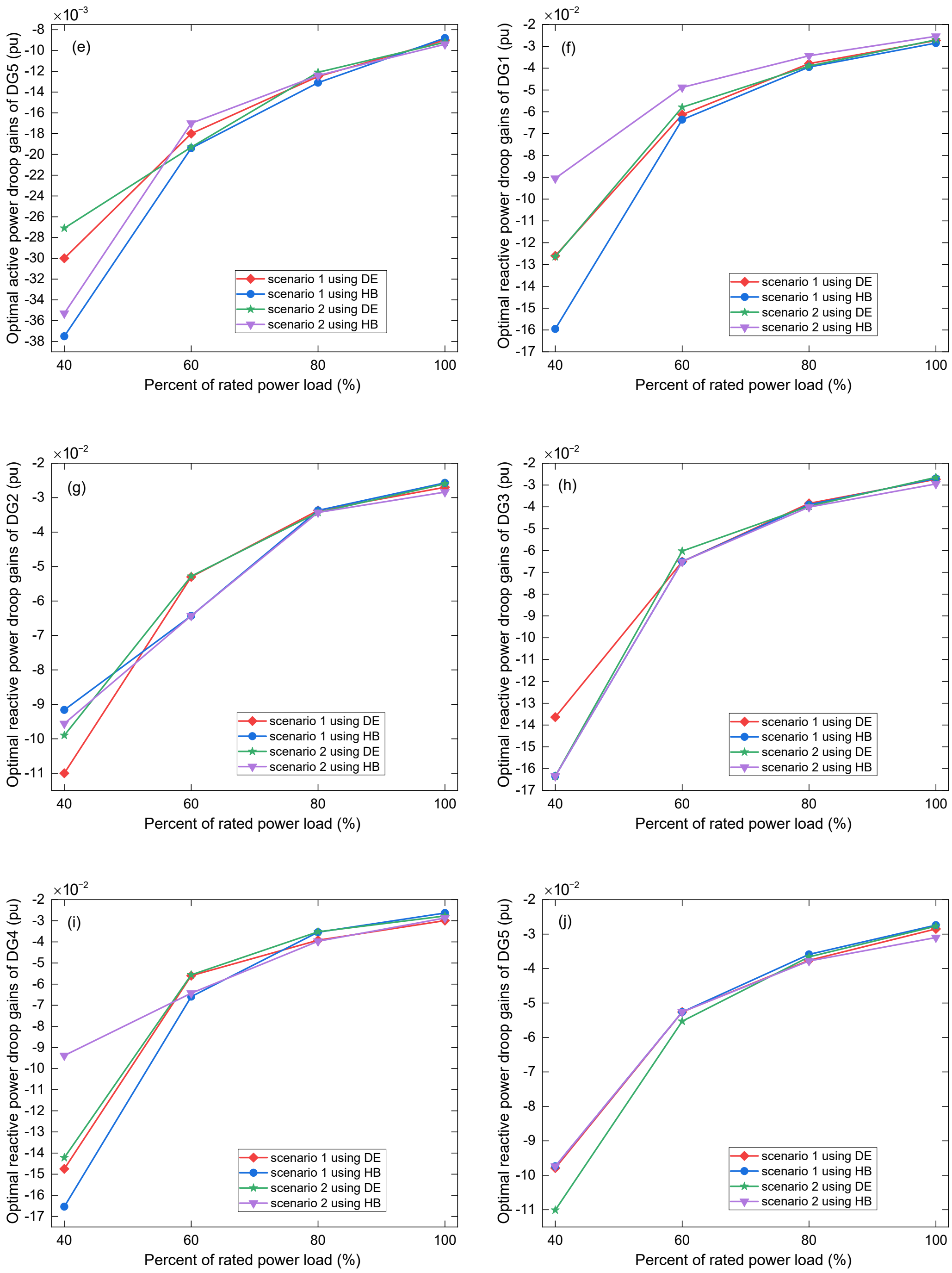

Fig. 1. Optimal droop gains of the five DGs for Scenarios 1 and 2: optimal active power droop gains of DGs 1–5 (a–e) and optimal reactive power droop gains of DGs 1–5 (f–j)

values shown in Figs. 1 and 2, as well as Tables 4 and 6, represent the control variables described in Section 2. The rated active and reactive powers generated by the DGs, based on these optimal values at the rated load, are presented in Tables 8 and 9.

Table 5 presents the optimal positioning of five DGs on the 33-bus AMG for Scenarios 3 and 4, as determined by each algorithm. The use of control variables to determine optimal DG locations contributed to a more substantial reduction in power losses in Scenarios 3 and 4 compared to Scenarios 1 and 2, as evidenced by the data presented in Tables 10 and 11. Furthermore, Tables 4 and 6 show the optimal values of the DG reference voltage magnitudes for Scenarios 2 and 4, obtained through each algorithm and based on the aforesaid load profile. These values played a crucial role in helping the AMG reduce power losses and minimise the total voltage deviation, as indicated in Tables 10 and 11. Moreover, they improved the voltage profile and VSI of the AMG, as shown in Figs. 3(a) and 3(b).

Table 7 shows the operating frequency on the AMG for the scenarios computed using the DE and HB algorithms. All frequency values listed in this table satisfy the given constraints. Meanwhile, Tables 8 and 9 provide the active and reactive powers generated by the DGs between the scenarios using each algorithm.

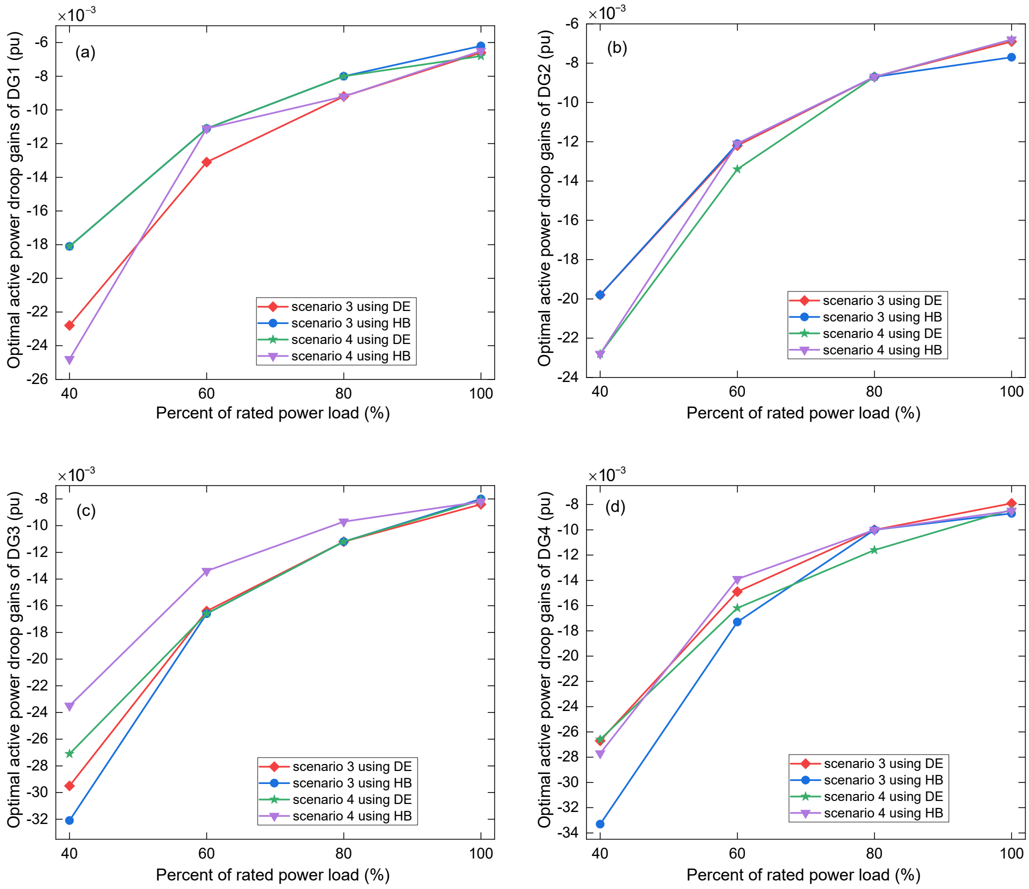

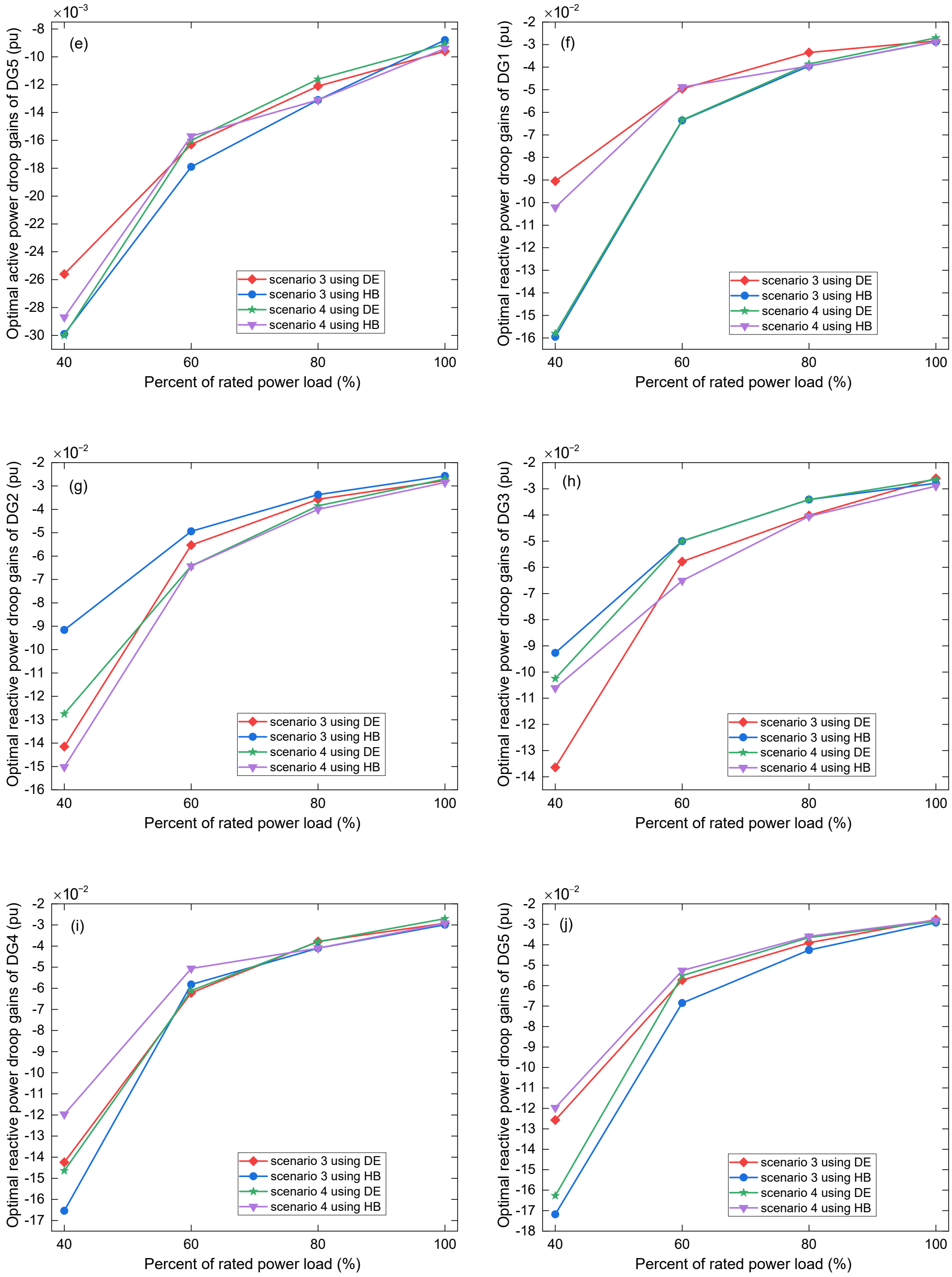

Fig. 2. Optimal droop gains of the five DGs for Scenarios 3 and 4: optimal active power droop gains of DGs 1–5 (a–e) and optimal reactive power droop gains of DGs 1–5 (f–j)

Table 5. The optimal placement (bus) of the DGs for Scenarios 3 and 4 using the DE and HB algorithms

Scenarios	3		4	
	DE	**HB**	**DE**	**HB**
DG1 (bus)	30	24	24	30
DG2 (bus)	3	26	26	19
DG3 (bus)	14	31	31	25
DG4 (bus)	25	14	2	6
DG5 (bus)	26	2	13	14

Table 6. Values $|V_{\text{ref}}|$ (pu) of DGs for Scenario 4 using the DE and HB algorithms

% rated load	DE					HB				
	DG1	**DG2**	**DG3**	**DG4**	**DG5**	**DG1**	**DG2**	**DG3**	**DG4**	**DG5**
40	1.0167	1.0178	1.0200	1.0188	1.0142	1.0188	1.0182	1.0057	1.0186	1.0136
60	1.0100	1.0179	1.0190	1.0122	1.0027	1.0200	1.0000	1.0000	1.0048	1.0000
80	1.0182	1.0199	1.0185	1.0086	1.0049	1.0200	1.0000	1.0128	1.0200	1.0000
100	1.0151	1.0158	1.0133	1.0106	1.0108	1.0151	1.0167	1.0171	1.0177	1.0123

Table 7. Values of the operating frequency (pu) for four scenarios

Scenarios	1		2		3		4		Base
% rated load	**DE**	**HB**	**DE**	**HB**	**DE**	**HB**	**DE**	**HB**	
40	0.9903	0.9900	0.9907	0.9902	0.9904	0.9901	0.9905	0.9900	–
60	0.9903	0.9900	0.9900	0.9901	0.9900	0.9900	0.9901	0.9910	–
80	0.9901	0.9900	0.9903	0.9900	0.9900	0.9902	0.9901	0.9902	–
100	0.9900	0.9903	0.9901	0.9900	0.9900	0.9900	0.9900	0.9900	0.9984

Table 10 compares the objective functions for the proposed model and the percentage of power losses in four scenarios, using two metaheuristic algorithms. As reported in [14], the allowed percentage of active power loss in the AMG ranges 0.5–1.5% of the rated load. The results in Table 10 reveal that Scenario 4, which used the HB algorithm, achieved the best (lowest) values for active and reactive power losses, with 19.20 kW and 17.45 kvar, respectively. In addition, Scenario 4 with the HB algorithm also obtained the best (lowest) percentage of active and reactive power losses, with 0.184% and 0.271%, respectively. Contrarily, Scenario 1 utilising the DE algorithm provided the worst (highest) values of power losses, and percentage of losses.

Table 8. Values of rated active powers (kW) of the five DGs for scenarios

Scenarios	**1**		**2**		**3**		**4**		**Base**
	DE	**HB**	**DE**	**HB**	**DE**	**HB**	**DE**	**HB**	
DG1	821.20	872.00	838.05	821.90	859.50	906.30	833.60	866.20	800.30
DG2	829.65	806.80	817.00	831.70	822.25	749.35	833.60	830.30	800.30
DG3	694.75	672.40	725.45	711.70	695.70	727.05	715.85	711.45	800.30
DG4	728.60	723.80	709.85	729.80	730.30	674.20	693.85	684.20	800.30
DG5	653.75	652.90	637.25	632.45	618.15	668.20	648.20	632.85	533.55

Table 9. Values of rated reactive powers (kvar) of the five DGs for scenarios

Scenarios	**1**		**2**		**3**		**4**		**Base**
	DE	**HB**	**DE**	**HB**	**DE**	**HB**	**DE**	**HB**	
DG1	461.25	425.20	466.45	454.20	519.45	460.55	504.85	520.00	1180.55
DG2	507.65	514.30	511.40	510.10	482.00	510.05	507.65	450.55	187.60
DG3	416.75	419.30	367.85	382.70	394.25	508.25	505.95	462.35	166.20
DG4	436.95	459.35	470.40	467.10	433.10	380.40	407.20	502.25	155.20
DG5	488.15	490.00	489.75	489.85	475.50	448.20	374.60	365.75	626.70

Table 10. Comparison of objective functions, percent of active power loss (percent of P_{loss}) and percent of reactive power loss (percent of Q_{loss}) for four scenarios using the DE and HB algorithms

Scenarios	F_1 (kW)		F_2 (kvar)		F_3 (pu)		Percent of P_{loss} (%)		Percent of Q_{loss} (%)	
	DE	HB	DE	HB	DE	HB	DE	HB	DE	HB
1	27.55	27.40	25.55	25.40	2.915	2.966	0.265	0.263	0.396	0.395
2	26.10	25.90	24.50	24.35	1.001	0.961	0.251	0.249	0.380	0.378
3	22.70	21.60	19.75	19.15	2.865	2.858	0.218	0.208	0.306	0.297
4	20.50	19.20	18.65	17.45	1.034	1.328	0.197	0.184	0.290	0.271

This table shows that the use of the proposed HB algorithm substantially minimises power losses in the AMG. Moreover, Scenario 2 using the HB algorithm achieved the best value to minimise the total voltage deviation, while Scenarios 1 and 3 provided the poorer values.

In the base scenario, the power losses at the rated load were 17.20 kW and 13.00 kvar, as shown in Table 11. Interestingly, this table also reveals that power losses were significantly minimised in Scenarios 1–4 compared to the base scenario, using both the DE and HB algorithms.

The best values for the power losses and the percentage of losses minimisation corresponded to Scenario 4 using the HB algorithm, while Scenario 1 with the DE and HB algorithms provided the worst values. Moreover, Scenarios 2 and 4 exhibited lower values of total bus voltage deviation compared to Scenarios 1 and 3, as well as the base scenario.

Table 11. Comparison of P_{loss} active power loss and Q_{loss} reactive power loss, % active power loss mitigation (% P_{loss} mitigation), % reactive power loss mitigation (% Q_{loss} mitigation), and total voltage deviation ΔV at the rated load for four scenarios

Scenarios		P_{loss} (kW)	% P_{loss} mitigation	Q_{loss} (kvar)	% Q_{loss} mitigation	ΔV (pu)
Base		17.20	–	13.00	–	0.634
1	**DE**	12.90	25.00	11.95	8.08	0.758
	HB	12.90	25.00	11.95	8.08	0.737
2	**DE**	12.60	26.74	11.55	11.15	0.255
	HB	12.45	27.62	11.50	11.54	0.257
3	**DE**	10.90	36.63	9.40	27.69	0.740
	HB	10.05	41.57	8.90	31.54	0.727
4	**DE**	10.10	41.28	9.05	30.38	0.281
	HB	10.00	41.86	8.90	31.54	0.231

Figures 3(a) and 3(b) depict the voltage profile and VSI, respectively, of the 33-bus AMG at the rated load for Scenarios 1–4 using the DE and HB algorithms. Scenario 4 using the HB algorithm had the best voltage profile and VSI. In contrast, Scenario 1 with the DE algorithm yielded the least desirable results. These figures show that the use of optimal parameters for

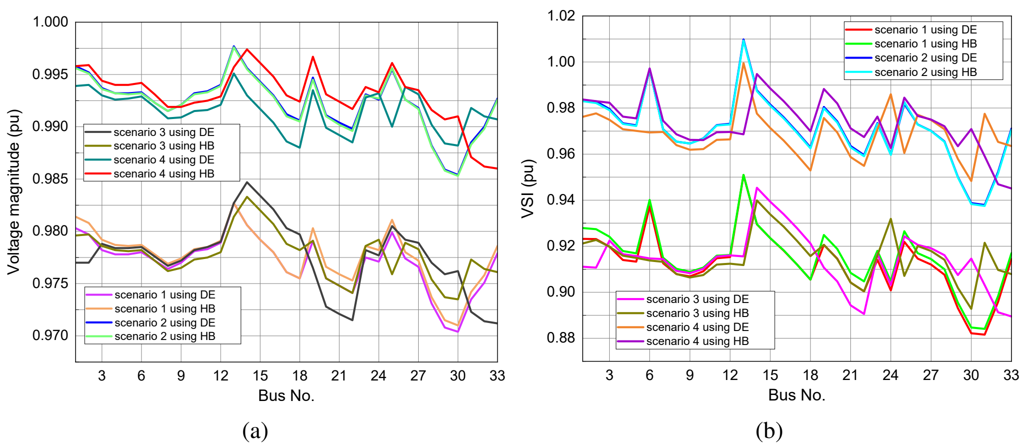

Fig. 3. Voltage profile (a) and VSI (b) of IEEE 33-bus AMG at the rated load

Table 12. Minimum nodal voltage magnitude (pu) and VSI (pu) of IEEE 33-bus AMG at the rated load for four scenarios using two metaheuristic algorithms

Scenarios	**1**		**2**		**3**		**4**		**Base**
	DE	**HB**	**DE**	**HB**	**DE**	**HB**	**DE**	**HB**	
$\lvert V_i \rvert$ (bus)	0.9704 (30)	0.9710 (30)	0.9854 (30)	0.9853 (30)	0.9712 (33)	0.9735 (30)	0.9880 (18)	0.9860 (33)	0.9733 (30)
VSI (bus)	0.8816 (31)	0.8841 (31)	0.9379 (31)	0.9375 (31)	0.8895 (33)	0.8928 (30)	0.9483 (30)	0.9451 (33)	–

DDGs helps to enhance the voltage profile and VSI. As shown in Table 12, the minimum bus voltage magnitude values for Scenarios 2 and 4 using the DE algorithm were higher than those for Scenarios 1 and 3 using the HB algorithm. The best VSI value was observed for Scenario 4 using the DE algorithm, while the worst was seen for Scenario 1, also using the DE algorithm.

7. Conclusions

In this study, the optimal droop gains and reference voltage magnitude of the five droop-controlled dispatchable DGs corresponding to their locations in the modified IEEE 33-bus AMG have been obtained using the HB algorithm. The objective functions were to mitigate active power loss considering the reduction of reactive power loss and the total nodal voltage deviation and the enhancement of VSI. The results achieved indicate that Scenario 4, utilising the HB algorithm, has produced the best values for minimising power losses. In addition, the total bus voltage deviation has been significantly reduced, as well as the VSI improvement, when the HB algorithm has been used. The HB algorithm is a flexible and effective technique that can be applied to AMGs with a larger number of buses.

The findings of this study have to be seen in light of some limitations. Three main shortcomings of this work need to be addressed in further research. First, this study was based on the assumption that only five dispatchable DGs were set on the system. Therefore, to improve the maximum benefits of installing dispatchable DGs in AMG, multiple dispatchable DGs with small capacity shall be installed with more than 30% of the total number of buses [37]. Second, to enhance the operational capability of AMG, the suitable size and location of dispatchable DGs and non-dispatchable DGs (e.g., wind turbines, solar plants, etc.), and energy storage systems (e.g., BESS) need to be resolved for further research. Lastly, the original DE and HB algorithms were designed to deal with optimisation problems for continuous variables. However, in this study, there have been continuous and discrete variables. For example, optimal droop gains and reference voltage magnitude variables of DGs have been continuous variables, whereas optimal placement of DGs in the system has been a discrete variable. Consequently, the modified DE and HB algorithms are significant in improving the heuristic capability in the search space, including continuous and discrete variables.

Acknowledgements

Tham X. Nguyen would like to express his deepest gratitude to the Governments of Vietnam and Poland for the financial support for his Ph.D. program at the Wrocław University of Science and Technology, Wrocław, Poland.

References

[1] Pepermans G., Driesen J., Haeseldonckx D., Belmans R., D'haeseleer W., *Distributed generation: definition, benefits and issues*, Energy policy, vol. 33, no. 6, pp. 787–798 (2005), DOI: 10.1016/j.enpol.2003.10.004.

[2] Lis R., Sobierajski M., *Integration of distributed resources in power systems*, Renewable Energy Systems, University of Technology, Wrocław (2011).

[3] Photovoltaics D.G., Storage E., *IEEE standard for interconnection and interoperability of distributed energy resources with associated electric power systems interfaces*, IEEE Std, pp. 1547–2018 (2018), DOI: 10.1109/IEEESTD.2018.8332112.

[4] Dos S.C.L., Mariani V.C., Leite J.V., *Solution of Jiles–Atherton vector hysteresis parameters estimation by modified Differential Evolution approaches*, Expert Systems with Applications, vol. 39, no. 2, pp. 2021–2025 (2012), DOI: 10.1016/j.eswa.2011.08.035.

[5] Basu M., *Dynamic optimal power flow for isolated microgrid incorporating renewable energy sources*, Energy, vol. 264, 126065 (2023), DOI: 10.1016/j.energy.2022.126065.

[6] Menna Allah El-sayed Mohamed El-Saeed, Abdel-Gwaad A.F., Farahat M.A., *Solving the capacitor placement problem in radial distribution networks*, Results in Engineering, vol. 17, 100870 (2023), DOI: 10.1016/j.rineng.2022.100870.

[7] Khoshayand H.A., Wattanapongsakorn N., Mahdavian M., Ganji E., *A new method of decision making in multi-objective optimal placement and sizing of distributed generators in the smart grid*, Archives of Electrical Engineering, pp. 253–271 (2023), DOI: 10.24425/aee.2023.143701.

[8] Bora T.C., Mariani V.C., Dos S.C.L., *Multi-objective optimization of the environmental-economic dispatch with reinforcement learning based on non-dominated sorting genetic algorithm*, Applied Thermal Engineering, vol. 146, pp. 688–700 (2019), DOI: 10.1016/j.applthermaleng.2018.10.020.

[9] Mukhopadhyay B., Das D., *Optimal multi-objective expansion planning of a droop-regulated islanded microgrid*, Energy, vol. 218, 119415 (2021), DOI: 10.1016/j.energy.2020.119415.

[10] Roy N.B., Das D., *Optimal allocation of active and reactive power of dispatchable distributed generators in a droop controlled islanded microgrid considering renewable generation and load demand uncertainties*, Sustainable Energy, Grids and Networks, vol. 27, 100482 (2021), DOI: 10.1016/j.segan.2021.100482.

[11] Kirthiga M.V., Daniel S.A., Gurunathan S., *A methodology for transforming an existing distribution network into a sustainable autonomous micro-grid*, IEEE Transactions on Sustainable Energy, vol. 4, no. 1, pp. 31–41 (2013), DOI: 10.1109/TSTE.2012.2196771.

[12] Uniyal A., Sarangi S., *Optimal DG allocation in a microgrid using droop-controlled load flow*, in Intelligent Computing Techniques for Smart Energy Systems, Springer, pp. 745–752 (2020), DOI: 10.1007/978-981-15-0214-9_77.

[13] Shaaban M.F., Saber A., Ammar M.E., Zeineldin H.H., *A multi-objective planning approach for optimal DG allocation for droop based microgrids*, Electric Power Systems Research, vol. 200, 107474 (2021), DOI: 10.1016/j.epsr.2021.107474.

[14] Gupta Y., Doolla S., Chatterjee K., Pal B.C., *Optimal DG allocation and Volt–Var dispatch for a droop-based microgrid*, IEEE Transactions on Smart Grid, vol. 12, no. 1, pp. 169–181 (2021), DOI: 10.1109/TSG.2020.3017952.

[15] Gupta Y., Nellikkath R., Chatterjee K., Doolla S., *Volt–Var Optimization and Reconfiguration: Reducing Power Demand and Losses in a Droop-Based Microgrid*, IEEE Transactions on Industry Applications, vol. 57, no. 3, pp. 2769–2781 (2021), DOI: 10.1109/TIA.2021.3057008.

[16] Moazami G.H., Kazemi M.H., *An optimal autonomous microgrid cluster based on distributed generation droop parameter optimization and renewable energy sources using an improved grey wolf optimizer*, Engineering Optimization, vol. 50, no. 5, pp. 819–839 (2018), DOI: 10.1080/0305215X.2017.1355970.

[17] Khalid M., Akram U., Shafiq S., *Optimal planning of multiple distributed generating units and storage in active distribution networks*, IEEE Access, vol. 6, pp. 55234–55244 (2018), DOI: 10.1109/ACCESS.2018.2872788.

[18] Foroutan V.B., Moradi M.H., Abedini M., *Optimal operation of autonomous microgrid including wind turbines*, Renewable Energy, vol. 99, pp. 315–324 (2016), DOI: 10.1016/j.renene.2016.07.008.

[19] Yazdavar A.H., Shaaban M.F., El-Saadany E.F., Salama M.M., Zeineldin H.H., *Optimal planning of distributed generators and shunt capacitors in isolated microgrids with nonlinear loads*, IEEE Transactions on Sustainable Energy, vol. 11, no. 4, pp. 2732–2744 (2020), DOI: 10.1109/TSTE.2020.2973086.

[20] Uniyal A., Sarangi S., *Optimal allocation of ELC in microgrid using droop controlled load flow*, IET Generation, Transmission & Distribution, vol. 13, no. 20, pp. 4566–4578 (2019), DOI: 10.1049/iet-gtd.2018.5174.

[21] Kreishan M.Z., Zobaa A.F., *Allocation of Dump Load in Islanded Microgrid Using the Mixed-Integer Distributed Ant Colony Optimization*, IEEE Systems Journal (2022), DOI: 10.1109/JSYST.2021.3100409.

[22] Hameed F., Al Hosani M., Zeineldin H.H., *A Modified Backward/Forward Sweep Load Flow Method for Islanded Radial Microgrids*, IEEE Transactions on Smart Grid, vol. 10, no. 1, pp. 910–918 (2019), DOI: 10.1109/TSG.2017.2754551.

[23] Hashim F.A., Houssein E.H., Hussain K., Mabrouk M.S., Al-Atabany W., *Honey Badger Algorithm: New metaheuristic algorithm for solving optimization problems*, Mathematics and Computers in Simulation, vol. 192, pp. 84–110 (2022), DOI: 10.1016/j.matcom.2021.08.013.

[24] Abdulqadder I.H., Zou D., Aziz I.T., *The DAG blockchain: A secure edge assisted honeypot for attack detection and multi-controller based load balancing in SDN 5G*, Future Generation Computer Systems, vol. 141, pp. 339–354 (2023), DOI: 10.1016/j.future.2022.11.008.

[25] Diab A.A.Z., Tolba M.A., El-Rifaie A.M., Denis K.A., *Photovoltaic parameter estimation using honey badger algorithm and African vulture optimization algorithm*, Energy Reports, vol. 8, pp. 384–393 (2022), DOI: 10.1016/j.egyr.2022.05.168.

[26] Akbari E., Shafaghatian N., Zishan F., Montoya O.D., Giral-Ramírez D.A., *Optimized Two-Level Control of Islanded Microgrids to Reduce Fluctuations*, IEEE Access, vol. 10, pp. 95824–95838 (2022), DOI: 10.1109/ACCESS.2022.3203730.

[27] Janjanam L., Saha S.K., Kar R., Mandal D., *Hammerstein-Wiener nonlinear system identification by using honey badger algorithm hybridized Sage-Husa adaptive Kalman filter with real-time applications*, AEU-International Journal of Electronics and Communications, vol. 151, 154218 (2022), DOI: 10.1016/j.aeue.2022.154218.

[28] Moradi M.H., Abedini M., *A novel method for optimal DG units capacity and location in Microgrids*, International Journal of Electrical Power & Energy Systems, vol. 75, pp. 236–244 (2016), DOI: 10.1016/j.ijepes.2015.09.013.

[29] Chakravorty M., Das D., *Voltage stability analysis of radial distribution networks*, International Journal of Electrical Power & Energy Systems, vol. 23, no. 2, pp. 129–135 (2001), DOI: 10.1016/S0142-0615(00)00040-5.

[30] Vasquez J.C., Guerrero J.M., Savaghebi M., Eloy-Garcia J., Teodorescu R., *Modeling, analysis, and design of stationary-reference-frame droop-controlled parallel three-phase voltage source inverters*, IEEE Transactions on industrial electronics, vol. 60, no. 4, pp. 1271–1280 (2013), DOI: 10.1109/TIE.2012.2194951.

[31] Price K.V., *Differential evolution: a fast and simple numerical optimizer*, in Proceedings of North American fuzzy information processing, pp. 524–527 (1996), DOI: 10.1109/NAFIPS.1996.534790.

[32] Kundur P.S., *Power System Stability and Control*, 1st edition, New York, McGraw Hill (1994).

[33] Lopes J.P., Moreira C.L., Madureira A.G., *Defining control strategies for microgrids islanded operation*, IEEE Transactions on power systems, vol. 21, no. 2, pp. 916–924 (2006), DOI: 10.1109/TPWRS.2006.873018.

[34] Al-Kaabi M., Al Hasheme J., Al-Bahrani L., *Improved Differential Evolution Algorithm to solve multi-objective of optimal power flow problem*, Archives of Electrical Engineering, vol. 71, no. 3 (2022), DOI: 10.24425/aee.2022.141676.

[35] Teng J.H., *A direct approach for distribution system load flow solutions*, IEEE Transactions on power delivery, vol. 18, no. 3, pp. 882–887 (2003), DOI: 10.1109/TPWRD.2003.813818.

[36] Baran M.E., Wu F.F., *Network reconfiguration in distribution systems for loss reduction and load balancing*, IEEE Transactions on Power delivery, vol. 4, no. 2, pp. 1401–1407 (1989), DOI: 10.1109/61.25627.

[37] Sivakumar K., Jayashree R., Danasagaran K., *Efficiency-driven planning for sizing of distributed generators and optimal construction of a cluster of microgrids*, Engineering Science and Technology, an International Journal (2021), DOI: 10.1016/j.jestch.2021.02.015.